Advances in Water Resources 167 (2022) 104286

Contents lists available at ScienceDirect

Advances in Water Resources

journal homepage: www.elsevier.com/locate/advwatres

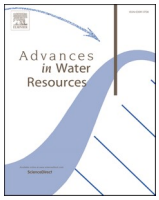

On the localization of chemical reactions in multicontinuum media

Jingjing Wang [a,b,c,d,*], Jesus Carrera [c,d], Maarten W. Saaltink [b,d], Cristina Valhondo [c,d,e]

[a] Department of Geotechnical Engineering, College of Civil Engineering, Tongji University, Shanghai 200092, China
[b] Department of Civil and Environmental Engineering, Universitat Politècnica de Catalunya (UPC), Jordi Girona 1-3, 08034 Barcelona, Spain
[c] Geosciences Department, Institute of Environmental Assessment and Water Research (IDAEA), Severo Ochoa Excellence Center, Spanish Council for Scientific Research (CSIC), c/ Jordi Girona, 20, 08034 Barcelona, Spain
[d] Associated Unit—Hydrogeology Group (UPC-CSIC), Jordi Girona, 08034 Barcelona, Spain
[e] Géosciences Montpellier, Université de Montpellier, CNRS, 300 Avenue Emile Jeanbrau, CC MSE, 34095 Montpellier, France

ARTICLE INFO

Keywords:
Chemical localization
Multirate mass transfer
Reactive transport
Multicontinuum media
Numerical modeling

ABSTRACT

Reactive transport (RT) through heterogeneous media, may cause chemical heterogeneity if water flux is slow through portions of the medium. In such cases, chemical localization (i.e., the occurrence of reactions that would not occur in well mixed media) may develop, which is especially relevant for biochemical reactions occurring in biofilms. The objective of this work is to study the conditions for chemical localization. We represent the impact of heterogeneity by means of the non-local multirate mass transfer (MRMT) model, which views the porous media as consisting of one mobile and many immobile zones. A dimensional analysis of the governing equations shows that the problem is characterized by reaction times and the distribution of residence times in immobile zones, relative to transport time. To analyze the interplay between them, we simulated simple RT problems in multicontinuum media. Results indicate that immobile zones with residence times much smaller than transport can be lumped together with the mobile zone by modifying the reaction rates, which reduces computations. More importantly, reactions driven by species that are not present in the inflowing water but are the result of previous reactions will take place preferentially in immobile zones, whose residence time is comparable to or larger than reaction times. In fact, daughter species may take a long time and distance to build up. That is, daughter species will not be largest near the inflow, where parent species display largest concentrations, but further downstream at isolated (long residence times) immobile zones.

1. Introduction

Reactive transport (RT) in porous media is essential for understanding environmental processes, such as the fate of contaminants in aquifers, and for a proper design and management of remediation strategies, such as managed aquifer recharge (e.g., Valhondo et al., 2020) or CO_2 geological storage (e.g., Agrawal et al., 2021). Carrera et al. (2022) argue that the basic problem of RT is how to address the chemical and physical heterogeneity of natural media.

Physical heterogeneity has received broad attention in the transport literature. It is well known that transport in heterogeneous porous media displays anomalous (non-Fickian) behavior (Kitanidis, 1988) both at field (Adams and Gelhar, 1992) and laboratory scales (Berkowitz and Scher, 2009; Levy and Berkowitz, 2003; Valocchi, 1985), displaying early arrivals, long tails and scale-dependent dispersion coefficients (Carrera, 1993). The problem is especially relevant for reactive transport because numerous reactions depend on local scale mixing. To overcome this problem, researchers have focused on small scale simulations in an attempt to simulate heterogeneity explicitly (e.g., Cirpka et al., 2015) or, even by pore scale simulations (e.g., Agrawal et al., 2021). Beyond the cost of such simulations, what emerges is that upscaling parameters does not suffice, but the transport equation may have to change and the advection-dispersion-reaction equation (ADRE) cannot be considered suitable for reactive transport (Carrera et al., 2022; Molins and Knabner, 2019; Soler-Sagarra et al., 2022).

Many non-local methods have been developed to address the need for an alternative transport equation. These include continuous time random walks (CTRW) (Berkowitz et al., 2006; Berkowitz and Scher, 1998; Dentz et al., 2015, 2004), fractional advection-dispersion equations (fADE) (Benson et al., 2000; Benson and Meerschaert, 2009; Marseguerra and Zoia, 2008; Schumer et al., 2003a, 2003b), multirate mass transfer (MRMT) (Babey et al., 2017; Benson and Meerschaert, 2009; Dentz et al., 2011; Fernandez-Garcia and Sanchez-Vila, 2015;

* Corresponding author.
E-mail addresses: jingjingwangxiang@126.com (J. Wang), jesus.carrera@cid.csic.es (J. Carrera), maarten.saaltink@upc.edu (M.W. Saaltink).

https://doi.org/10.1016/j.advwatres.2022.104286
Received 30 March 2022; Received in revised form 10 July 2022; Accepted 26 July 2022
Available online 28 July 2022

Nomenclature

α	Mass transfer rate, $[T^{-1}]$
$f(\alpha)$	Probability density function of mass transfer rates
$\tau_\alpha \equiv 1/\alpha$	Residence time, [T]
$P(\tau_\alpha)$	Probability density function of residence times
α_0	Scale parameter of $f(\alpha)$
τ_{α_0}	Scale parameter of $P(\tau_\alpha)$
β	Shape parameter of $f(\alpha)$ and $P(\tau_\alpha)$
$\Gamma(\beta)$	Gamma function
c_m	Concentrations in the mobile zone, $[ML^{-3}]$
c_{im}	Concentrations in the immobile zones, $[ML^{-3}]$
ϕ_m	Porosity of mobile zone, [-]
ϕ_{im}	Porosity of immobile zones, [-]
$\mathbf{q}$	Darcy flux, $[LT^{-1}]$
$\mathbf{D}$	Hydrodynamic dispersion, $[L^2T^{-1}]$
r_m	Sink-source term due to chemical reactions in the mobile zone, $[ML^{-3}T^{-1}]$
r_{im}	Sink-source term in the immobile zones, $[ML^{-3}T^{-1}]$
k_m	Reaction rate constant in the mobile zone, $[T^{-1}]$
$k_{im}(\tau_\alpha)$	Local reaction rate constant in the immobile zone with τ_α, $[T^{-1}]$
$\tau_r \equiv 1/k_{im}(\tau_\alpha)$	Reaction time in the immobile zone with τ_α, [T]
$g(t)$	Memory function
$\kappa(t)$	Reaction rate kernel
$\delta(t)$	Dirac delta function
L_c	Characteristic length, [L]
t_c	Characteristic time, [T]
c_c	Characteristic concentration, $[ML^{-3}]$
q	Modulus of $\mathbf{q}$, $[LT^{-1}]$
D	Longitudinal component of $\mathbf{D}$, $[L^2T^{-1}]$
$v = q/\phi_m$	Mean fluid velocity in mobile zone, $[LT^{-1}]$
c_{mD}	Dimensionless concentrations in mobile zone ($c_{mD} = c_m/c_c$), [-]
c_{imD}	Dimensionless concentrations in immobile zones ($c_{imD} = c_{im}/c_c$), [-]
x_D	Dimensionless distance ($x_D = x/L_c$), [-]
t_D	Dimensionless time ($t_D = t/t_c$), [-]
η	Ratio of total immobile to mobile porosity ($\eta = \phi_{im}/\phi_m$), [-]
$\tau_{\alpha D}$	Dimensionless residence time ($\tau_{\alpha D} = \tau_\alpha/t_c$), [-]
τ_{rD}	Dimensionless reaction time ($\tau_{rD} = \tau_r/t_c$), [-]
c_e	Concentration of the inflowing water, $[ML^{-3}]$
$c^P_{m,1}$	Mobile concentration in the first node for the pulse injection, $[ML^{-3}]$
L	Travel distance of solute, [L]
t_A	Advective transport time, [T]
$\phi = \phi_m + \phi_{im}$	Total porosity, [-]
$\mathscr{L}\{\}(s)$	Laplace transform
s	Complex Laplace variable

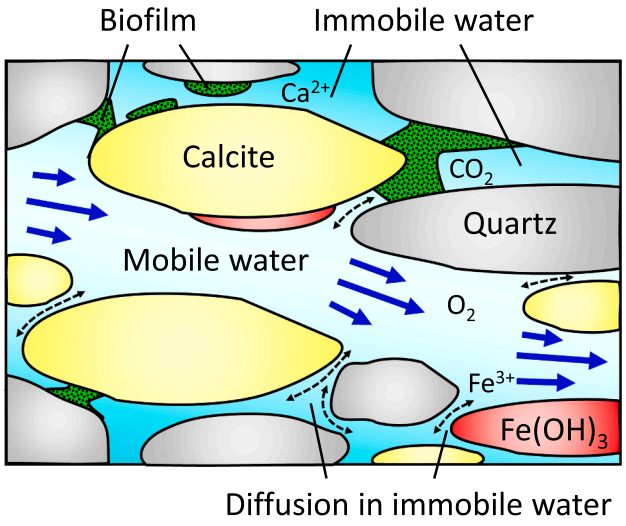

Fig. 1. Illustration of chemical localization: water flux tends to concentrate on a small fraction of the medium (blue arrows), often representing a small fraction of the reacting surfaces within a possible REV (Representative Elementary Volume). Proper mass balance requires model concentrations to be those of the flowing water, while some reactions may be localized in non-flowing portions of the pore space. The problem is especially relevant for biochemical reactions that occur in biofilms (green areas), possibly under redox conditions different from those of the mobile water.

Haggerty and Gorelick, 1995; Salamon et al., 2006; Wang et al., 2005), multiple interacting continua (MINC) (De Dreuzy et al., 2013; Pruess and Narasimhan, 1985), structured interacting continua (SINC) (Babey et al., 2015; Rapaport et al., 2017), memory functions (Carrera et al., 1998; Gouze et al., 2008; Haggerty et al., 2000; Willmann et al., 2008) and so forth. Although these methods use different approaches, they are essentially equivalent (Dentz and Berkowitz, 2003; Neuman and Tartakovsky, 2009; Silva et al., 2009). Unfortunately, their solution is often based on Laplace transform methods, which makes them poorly suited for multicomponent and/or non-linear RT. Therefore, most work on non-local methods deals with the behavior of breakthrough curves (BTCs) and conservative transport in heterogeneous porous media (Berkowitz and Scher, 2009; Dentz et al., 2015; Haggerty et al., 2000; Schumer et al., 2003b; Willmann et al., 2008). Still, MRMT, which can be considered the simplest paradigm of non-local transport methods, can be used for multicomponent RT. The medium is viewed as consisting of a mobile and several overlapping immobile zones. Each of these zones can be modeled numerically, which facilitates general RT simulation (Babaei and Islam, 2018; Massoudieh and Dentz, 2020; Soler-Sagarra et al., 2016; Willmann et al., 2010).

Chemical heterogeneity has received a lot less attention than physical heterogeneity. Chemical heterogeneity may refer to large scale variability, usually known from geological understanding, or to pore scale variability. Portions of the porous media, grain aggregates or individual grains or portion of grains can have different mineral compositions, leading to different reaction rates and different concentrations at different parts of the pore space. Furthermore, pore scale variability, causes water fluxes to be spatially variable, which causes dispersion and affects solute transport. Areas with low water flux may develop chemical conditions different from those of high flux, which carry most of the water (Fig. 1). In fact, reacting surface tend to be larger in low flux than in high flux areas. That is, physical heterogeneity may induce chemical heterogeneity. Steefel et al. (2005) call microenvironments these parts of the domain. We term the phenomenon chemical localization to emphasize the local occurrence of reactions. Furthermore, heterogeneity can cause chemical localization, i.e., the occurrence of reactions that would not occur in well mixed media.

The importance of chemical localization has been widely recognized in the literature. The discrepancy between measured mineral dissolution rates in laboratory and field is attributed to heterogeneity (Li et al., 2008). Modeling studies, sometimes combined with chemical and geophysical datasets, have shown the effect of heterogeneity on many particular systems, such as bioremediation of contaminated aquifers (Scheibe et al., 2006), reactive transport processes in fractures (Deng and Spycher, 2019) and mineral precipitation and dissolution in

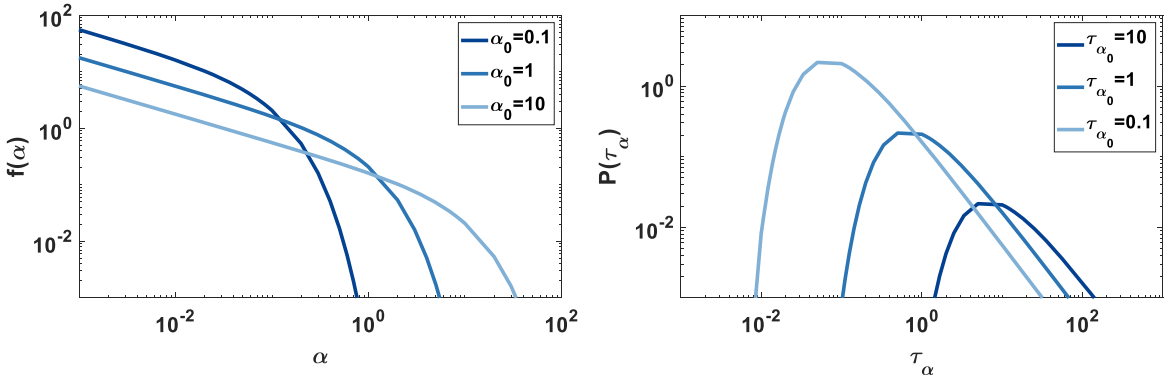

Fig. 2. Pdf of mass exchange rates, α (Gamma distibution), and residence times, τ_α, plotted in log-log scale for several values of $\tau_{\alpha 0}$ and $\beta = 1/2$. Note that the maximum of the latter is around $\tau_{\alpha 0}$ (the mode is $\tau_{\alpha 0}/(\beta+1)$ and the expected value $\tau_{\alpha 0}/(1-\beta)$). Its slope at large τ_α is $\beta+1$.

caprocks for CO2 storage (Tian et al., 2019). A clear example of chemical localization is presented by Luquot et al. (2016), who observed carbonate precipitation during injection of acidic CO2 brine into a shale core, which would not be possible if the acidic conditions associated to CO2 injection prevailed throughout the domain. Soler-Sagarra et al. (2016) showed that silicates weathering may cause sufficient alkalinity to facilitate carbonate precipitation in areas of low water flux. A similar situation may occur for biochemical reactions, which take place in biofilms. Biofilm growth generates immobile zones with limited access to electron acceptors, which facilitates the occurrence of reducing conditions (Bellin et al., 2014). The net result is that the microbial community is heterogeneous and reactions that would only occur under anaerobic conditions take place despite the overall aerobic water flux. In analyzing this problem, Dentz et al. (2011) concluded that transport under physical and chemical heterogeneity cannot be upscaled separately: upscaling reactions depends on physical heterogeneity and upscaling transport is affected by chemical heterogeneity. A similar conclusion was reached by Battiato et al. (2009). Furthermore, macroscale transport may be determined by microscale transport process in immobile zones (Gouze et al., 2008).

The situation cannot be considered satisfactory. On the one hand, chemical localization is frequently observed and we conjecture that its importance will increase with the need to simulate biochemical RT (Carrera et al., 2022). Yet, it is not clear how to upscale the processes. What is clear is that a multicontinuum representation is needed to be able to host and represent different chemical environments. In fact, Lichtner and Kang (2007) adopted a lattice Boltzmann solution method with this goal. We contend that a MRMT representation can reach the same goal at a much lower cost. Still, the problem has never been analyzed formally, so that numerous questions need to be answered regarding the conditions for localization and when does it need to be modeled.

The objective of this work is to study the conditions for localization of reactions in MRMT RT formulations. To do so, first, we establish the governing equations of reactive transport in multicontinuum media and deduce a dimensionless form of these equations. We then use the resulting model in two simple cases to analyze the conditions for localization.

2. Methodology

We model reactive transport in heterogeneous porous medium using the MRMT approach (Haggerty and Gorelick, 1995). Every point (representative elementary volume) is viewed as consisting of a mobile zone and a distribution of immobile zones characterized by their residence times. Each immobile zone exchanges solute mass with the mobile zone proportionally to the mass transfer rate, α [T^{-1}] (a complete description of variables employed in this paper is given in the Nomenclature). Therefore, it is natural to characterize this distribution by a probability density function (pdf) of mass transfer rates, $f(\alpha)$ (see Fig. 2 left). To facilitate comparison to other non-local methods, we also characterize immobile zones by the distribution, $P(\tau_\alpha)$, of residence times, $\tau_\alpha \equiv 1/\alpha$ [T] (Haggerty et al., 2004) (see Fig. 2 right). $P(\tau_\alpha)$ is given by (Dentz et al., 2015, 2011; Dentz and Berkowitz, 2003)

$$P(\tau_\alpha) = \tau_\alpha^{-2} f(\alpha) = \frac{\tau_{\alpha_0}^{\beta}}{\Gamma(\beta)} \frac{1}{\tau_\alpha^{\beta+1}} e^{-\frac{\tau_{\alpha_0}}{\tau_\alpha}} \tag{1}$$

where β is the shape parameter, τ_{α_0} is the scale parameter, and Γ(β) is the Gamma function. The residence time probability $P(\tau_\alpha)d\tau_\alpha$ is the immobile zones frequency with residence times in the interval $[\tau_\alpha, \tau_\alpha + d\tau_\alpha]$. Obviously, it satisfies the condition $\int_0^\infty P(\tau_\alpha)d\tau_\alpha = 1$.

2.1. Governing equations

The transport of any reactive species in a medium that consists of a mobile continuum and multiple immobile continua can be expressed as (Dentz et al., 2011; Donado et al., 2009; Willmann et al., 2010)

$$\phi_m \frac{\partial c_m}{\partial t} = L_t[c_m] - \phi_{im} \int_0^\infty \frac{1}{\tau_\alpha} P(\tau_\alpha)[c_m(x,t) - c_{im}(x,\tau_\alpha,t)]d\tau_\alpha + \phi_m r_m \tag{2}$$

where $L_t[c_m] = -[\mathbf{q}\cdot\nabla c_m] + \nabla\cdot[\phi_m \mathbf{D}\cdot\nabla c_m]$ is the transport operator that describes advection and dispersion, $\mathbf{q}$ [LT^{-1}] is Darcy flux, $\mathbf{D}$ [L^2T^{-1}] is the hydrodynamic dispersion tensor; ϕ_m [-] and ϕ_{im} [-] are the porosities of mobile and immobile zones, which denote the volume fraction of mobile pore and immobile pore water over the bulk volume, respectively; c_m [ML^{-3}] and c_{im} [ML^{-3}] are concentrations in the mobile and immobile zone, which are expressed as mass per unit volume of mobile and immobile water, respectively; r_m [$ML^{-3}T^{-1}$] is the sink-source term due to chemical reactions in the mobile zone and corresponds to the mass removed by reactions in the mobile zone per unit volume of mobile water per unit time. It should be noted that Eq. (2) remains valid for sorbing solutes, in which case ϕ_m and ϕ_{im} are the storage capacity (porosity times local retardation coefficient) of mobile and immobile zones, respectively.

Mass balance in each immobile zone is given by

$$\frac{\partial c_{im}(x,\tau_\alpha,t)}{\partial t} = \frac{1}{\tau_\alpha}[c_m(x,t) - c_{im}(x,\tau_\alpha,t)] + r_{im}(x,\tau_\alpha,t) \tag{3}$$

where r_{im} [$ML^{-3}T^{-1}$] is the reactions sink-source term in the immobile zone with residence time τ_α, which corresponds to the mass removed by reactions in the immobile zone per unit volume of immobile water per unit time.

Mass exchange between mobile and immobile zones is modeled by a first-order mass transfer term, represented by the continuous variable τ_α

and characterized by a distribution density function $P(\tau_\alpha)$ for the immobile zones. Thus, the total mass exchange is the weighted sum over all immobile zones as expressed in the integral term of Eq. (2). Integrating Eq. (3) with weight $P(\tau_\alpha)$ over τ_α, multiplying by ϕ_{im}, and substituting it into Eq. (2), yields the total solute mass balance,

$$\phi_m \frac{\partial c_m(x,t)}{\partial t} + \phi_{im} \int_0^\infty P(\tau_\alpha) \frac{\partial c_{im}(x,\tau_\alpha,t)}{\partial t} d\tau_\alpha = L_t[c_m(x,t)] + r(x,t) \tag{4}$$

in which, r is the total reaction rate (now per unit volume of bulk porous medium) that integrates reactions in both mobile and immobile zones, i.e.,

$$r(x,t) = \phi_m r_m(x,t) + \phi_{im} \int_0^\infty P(\tau_\alpha) r_{im}(x,\tau_\alpha,t) d\tau_\alpha \tag{5}$$

If the reaction follows first-order kinetics, the reaction rate in the mobile zone will be

$$r_m(x,t) = -k_m c_m(x,t) \tag{6}$$

where k_m [T^{-1}] is the reaction rate constant. Similarly, the local reaction rate in the τ_α immobile zone becomes

$$r_{im}(x,\tau_\alpha,t) = -k_{im}(\tau_\alpha) c_{im}(x,\tau_\alpha,t) \tag{7}$$

where $k_{im}(\tau_\alpha)$ [T^{-1}] is the local reaction rate constant. The reaction time, $\tau_r \equiv 1/k_{im}(\tau_\alpha)$ [T], is assumed to depend on the immobile zone. This dependence should be understood as indicating that, as suggested by Fig. 1, different reactions with different reaction rates may occur in different immobile zones.

By inserting Eq. (7) into Eq. (3), then solving Eq. (3), we obtain the concentration in the immobile zone of τ_α as a function of mobile concentration history

$$c_{im}(x,\tau_\alpha,t) = c_{im}(x,\tau_\alpha,t=0) e^{-\left[\frac{1}{\tau_\alpha}+\frac{1}{\tau_r}\right]t} + \int_0^t \varphi(t-t') c_m(x,t') dt' \tag{8}$$

where $\varphi(t)$ is given by

$$\varphi(t) = \frac{1}{\tau_\alpha} e^{-\left[\frac{1}{\tau_\alpha}+\frac{1}{\tau_r}\right]t} \tag{9}$$

Assuming that the initial concentration in the immobile zones is zero (i.e., $c_{im}(x,\tau_\alpha,t=0)=0$), then by substituting Eq. (8) into Eq. (2) and rearranging terms, we obtain the total solute mass balance, as a sole function of c_m

$$\phi_m \frac{\partial c_m(x,t)}{\partial t} + \phi_{im} \frac{\partial}{\partial t} \int_0^t g(t-t') c_m(x,t') dt' = L_t[c_m(x,t)] - \int_0^t \kappa(t-t') c_m(x,t') dt' \tag{10}$$

where the memory function (Carrera et al., 1998; Haggerty et al., 2000) and reaction rate kernel (Dentz et al., 2011) are given by

$$g(t) = \int_0^\infty P(\tau_\alpha) \varphi(t) d\tau_\alpha \tag{11}$$

and

$$\kappa(t) = \phi_m(x) \frac{1}{\tau_{r,m}} \delta(t) + \phi_{im}(x) \int_0^\infty \frac{1}{\tau_r} P(\tau_\alpha) \varphi(t) d\tau_\alpha \tag{12}$$

respectively, in which $\delta(t)$ is the Dirac delta function. The memory function can be viewed as the rate of change of concentration in the immobile zone that is caused by a unit change of concentration in the mobile zone at initial time $t=0$. In the presence of reactions, the memory function not only incorporates the distribution of local mass transfer rates but also the distribution of local reaction rates. Similarly, the reaction rate kernel represents the local reactions in immobile zones: it integrates the reactions in both mobile and immobile zones, and accounts for the mass transfer between mobile and immobile zones.

Although the memory function is mainly controlled by the distribution of residence times in immobile zones, it is also affected by the local reaction times in immobile zones through $\varphi(t)$ (Eq. (9)). Likewise, the reaction rate kernel is mainly controlled by the chemical reactions, but it is also affected by the distribution of residence times in immobile zones. Clearly, the governing equations of reactive transport under physical and chemical heterogeneity (10), (11) and (12) are controlled by the distribution of residence times and reaction times in immobile zones simultaneously. The physical and chemical heterogeneities interact with each other, and together they govern reactive transport (Dentz et al., 2011).

2.2. Dimensionless formulations

We write the dimensionless form of Eqs. (10), (11)) and (12) using the definitions of Carrera et al. (2022), which allows us to avoid the need for a Peclet Number, so that all characteristic variables will be those describing the immobile zones distribution and reaction rates. Thus, we define the characteristic length

$$L_c = \frac{\phi_m D}{q} \tag{13}$$

where q is the modulus of $\mathbf{q}$ and D is any norm of $\mathbf{D}$ (here its longitudinal component). And, the characteristic transport time

$$t_c = \frac{L_c}{v} = \frac{\phi_m^2 D}{q^2} \tag{14}$$

Note that in 1D, the characteristic length equals the longitudinal dispersivity α_L if molecular diffusion is neglected in the mobile zone, because dispersion becomes $D = \alpha_L v$, where $v = q/\phi_m$ is the mean fluid velocity in the mobile zone. Using these definitions to write all variables in dimensionless form (i.e., $t_D = t/t_c$, $\tau_{\alpha D} = \tau_\alpha/t_c$, $x_D = x/L_c$, $c_{mD} = c_m/c_c$, etc.) and defining $\eta = \phi_{im}/\phi_m$ (see the nomenclature table at the end for the definition of all variables) and substituting them into Eq. (10), leads after some tedious but conventional algebra to the dimensionless form of the governing equations

$$\frac{\partial c_{mD}}{\partial t_D} + \eta \frac{\partial}{\partial t_D} \int_0^{t_D} g(t_D - t_D') c_{mD}(t_D') dt_D' = -\nabla_D c_{mD} + \nabla_D^2 c_{mD} - \int_0^{t_D} \kappa(t_D - t_D') c_{mD}(t_D') dt_D' \tag{15}$$

Note that in this dimensionless formulations, the physical and chemical heterogeneity are represented by the distribution of residence and reaction times (relative to the characteristic transport time t_c), and they are reflected simultaneously in the memory function and reaction rate kernel.

Obviously, in the situation where the characteristic length L_c and the dimensionless ratio of porosity of immobile zone to porosity of mobile zone η are invariable, the solution of Eq. (15) is governed by two characteristic dimensionless times, the dimensionless residence time $\tau_{\alpha D}$ (and its distribution) and the dimensionless reaction time τ_{rD} in immobile zones.

The solution of governing Eq. (15) in Laplace domain is expressed as

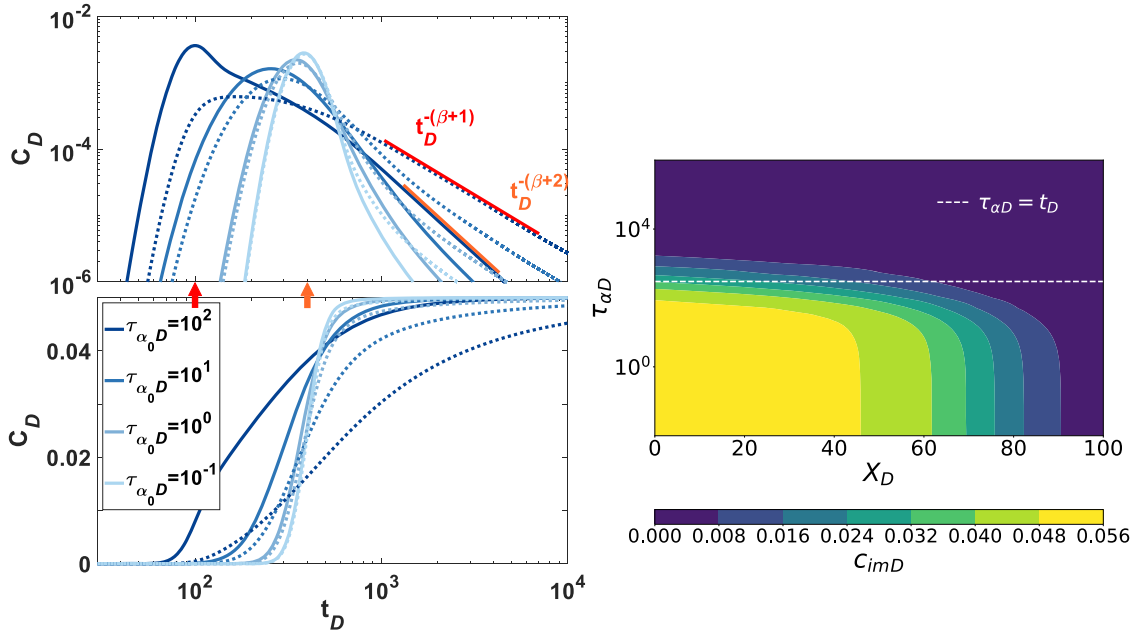

Fig. 3. Mobile (solid lines) and average immobile concentrations (dash lines) versus time (left column) at $x_D = 100L_c$ in response to a pulse injection (left top row) and to a continuous injection (actually, cumulative concentration) (left bottom row) for transport of a conservative species in a medium with a gamma distribution of residence times in immobile zones with $\beta = 1/2$, $\tau_{\alpha_0 D} = 10^2$, 10^1, 10^0, and 10^{-1}. The BTC peaks at the mobile advective time ($t_{AD} = 100$, red arrow) for slow exchange (i.e., large $\tau_{\alpha_0 D}$), but at the full porosity advective time ($t_{AD} = 400$, orange arrow) when exchange is fast, which also reduces the time it takes for immobile zones to equilibrate with inflow water. Cumulative concentration profile (colored, right column) versus dimensionless distance and dimensionless residence times (pdf with $\beta = 1/2$ and $\tau_{\alpha_0 D} = 10^{-1}$) at $t_D = 300$. The white dash line indicates the immobile zone whose residence time equals the travel time t_D. Note that immobile concentrations tend to mobile concentrations for $\tau_{\alpha D} < t_D$.

$$\mathscr{L}\{c_{mD}\}(s) = exp\left[\frac{x_D}{2}\left(1 - \sqrt{1 + 4[s[1 + \eta\mathscr{L}\{g\}(s)] + \mathscr{L}\{\kappa\}(s)]}\right)\right] \quad (16)$$

where $\mathscr{L}\{\cdot\}(s)$ represents the Laplace transform of a function. The Laplace transform of the memory function and reaction rate kernel are defined as

$$\mathscr{L}\{g\}(s) = \int_0^\infty P(\tau_{\alpha D})\mathscr{L}\{\varphi\}(s)d\tau_{\alpha D} \quad (17)$$

and

$$\mathscr{L}\{\kappa\}(s) = \frac{1}{\tau_{r,m_D}} + \eta\int_0^\infty \frac{1}{\tau_{rD}}P(\tau_{\alpha D})\mathscr{L}\{\varphi\}(s)d\tau_{\alpha D} \quad (18)$$

in which, the Laplace transform of $\varphi(t_D)$ is given by

$$\mathscr{L}\{\varphi\}(s) = \frac{\frac{1}{\tau_{\alpha D}}}{\frac{\tau_{\alpha D}+\tau_{rD}}{\tau_{\alpha D}\tau_{rD}} + s} \quad (19)$$

If we substitute s for $s[1 + \eta\mathscr{L}\{g\}(s)] + \mathscr{L}\{\kappa\}(s)$ in Eq. (16), then Eq. (16) becomes the solution of the transport equation in homogeneous media. Obviously, the retardation of localized physical heterogeneity on transport is reflected in the term $s\eta\mathscr{L}\{g\}(s)$, and the decay of localized chemical heterogeneity on reactive species is shown in the term $\mathscr{L}\{\kappa\}(s)$.

2.3. Steady state analytical solution

A steady state solution is possible for the continuous injection (or cumulative concentration of the pulse injection). The relevant output for the chemical localization problem is the ratio between the species concentrations in immobile and mobile zone, given by

$$\int_0^\infty c_{imD}(x_D, \tau_{\alpha D}, t_D)dt_D \Big/ \int_0^\infty c_{mD}(x_D, t_D)dt_D = \mathscr{L}\{\varphi\}(s)|_{s=0} \quad (20)$$

as can be obtained from the Laplace transform of Eqs. (8) and Eq. (9).

The concentration in the immobile zone is the weighted integral of concentrations in all immobile zones, which is defined as

$$c_{imD}(x_D, t_D) = \int_0^\infty P(\tau_{\alpha D})c_{im}(x_D, \tau_{\alpha D}, t_D)d\tau_{\alpha D} \quad (21)$$

From Eq. (8), we can obtain that

$$c_{imD}(x_D, t_D) = \int_0^{t_D} g\left(t_D - t_D^{'}\right)c_m\left(x_D, t_D^{'}\right)dt_D^{'} \quad (22)$$

Then, the ratio between the cumulative concentrations in the immobile and mobile zone becomes

$$\int_0^\infty c_{imD}(x_D, t_D)dt_D \Big/ \int_0^\infty c_{mD}(x_D, t_D)dt_D = \mathscr{L}\{g\}(s)|_{s=0} \quad (23)$$

3. Numerical models

We have built several numerical models to study chemical localization in physical and chemical heterogeneous media. The models have been calculated by the code RT_MRMT_DSA (Wang et al., 2022), which is an object-oriented FORTRAN2003 code based on finite element method (FEM) and capable of simulating reactive transport in multi-continuum media with MRMT. Species transport and reactions are solved simultaneously by using the Direct Substitution Approach (DSA), based on the Newton-Raphson method (Saaltink et al., 2001; Yeh and Tripathi, 1989).

All the models are one-dimensional with $\phi_m = 0.1$ [-], $\phi_{im} = 0.3$ [-], $\alpha_L = 1$ [L], $q = 1$ [LT^{-1}]. Thus, we have $L_c = 1$ [L], $t_c = 0.1$ [T], $\eta = 3$. The length of the domain $L = 100L_c$, and the simulated time $T = 10^4 t_c$. The mesh size $\Delta x = 1$ (i.e., $\Delta x_D = L_c$), and the time interval $\Delta t = 0.1$ (i.e., $\Delta t_D = 10 t_c$).

At the inlet, we set a Cauchy boundary condition

$$\begin{aligned} &D\nabla c_m(0,t)\cdot\mathbf{n} = q[c_e - c_m(0,t)], \quad q\cdot\mathbf{n} < 0 \\ &c_e = \delta(t) \end{aligned} \tag{24}$$

where c_e is the concentration of the inflowing water. The outlet is an open boundary condition

$$D\nabla c_m(L,t)\cdot\mathbf{n} = 0, \quad q\cdot\mathbf{n} \geq 0 \tag{25}$$

where$\mathbf{n}$ is a unit vector which is normal to the boundary, and $\cdot$ represents the inner product operator.

Initial concentrations are set to zero in both mobile and immobile zones, that is $c_m(x,0) = c_{im}(x,\tau_\alpha,0) = 0$ [ML^{-3}], except for the first mobile node that has initial concentration $c_{m,1} = 1$ [ML^{-3}]. This simulates a pulse injection.

In addition, we calculate the cumulative concentration $\int_0^t c dt$ for both mobile and immobile zones, which is equivalent to a continuous injection, simulated through a Cauchy boundary condition at the inlet (Eq. (24)) with an inflow concentration, $c_e = c_{m,1}\Delta x\phi_m/2q = 0.05$.

We simulate three cases: a no reaction system (conservative transport), a single reaction system and a sequential reaction system. Unless specified otherwise, models use the same gamma distribution of residence times with $\beta = 1/2$ and $\tau_{\alpha_0 D} = 10$.

In the single reaction system, only one hypothetical reaction $A \rightarrow B$ occurs, following a first-order rate law with $r_{k1} = k_1 c_A$. Thus, the degradation of species A follows $r_A = -k_1 c_A$, and the formation of species B, $r_B = k_1 c_A$. In the sequential reaction system, a second hypothetical reaction $B \rightarrow C$ is added, also with first-order kinetics, $r_{k2} = k_2 c_B$. Thus, the degradation of species A follows $r_A = -k_1 c_A$, the formation and degradation of species B, $r_B = k_1 c_A - k_2 c_B$, and the formation of species C, $r_C = k_2 c_B$. These are simple linear rate laws. In more realistic models rate laws may be more complex (Carrera et al., 2022). Also, the reaction rate coefficient can be different for each immobile (e.g., immobile zones with long residence times may tend to display more reducing conditions when simulating biochemical reactions). Eq. (7) expresses this dependence by writing $k_{im}(\tau_\alpha)$. Nevertheless, this study focuses on the localization of chemical reactions. Therefore, to facilitate comprehension we used simple reactions with constant rate coefficients ($k_{im}(\tau_\alpha) \equiv k_{im}$), although our code can handle more complicated reactions with variable rate coefficients.

4. Results and discussions

We discuss the results for conservative transport (Section 4.1), which provides the basis for understanding chemical localization in single (Section 4.2), and sequential (Section 4.3) reaction systems.

4.1. No reaction system

The impact of MRMT on conservative transport is well-known (e.g., Haggerty and Gorelick, 1995). We summarize here its main features to facilitate understanding the reactive case. Fig. 3 displays concentrations in both mobile and immobile zones in log scale for a pulse injection, and arithmetic scale for continuous injection. The log-log scale is usually preferred for tracer test analysis, because it emphasizes tailing. The late time slope of the pulse BTC is that of the memory function plus 1 (e.g., Haggerty et al., 2000). Therefore, by analyzing the BTC of conservative tracers, modelers can gain insight into the distribution of immobile zones. Still, solute remains in the immobile zones far longer, diffusing slowly back to the mobile zone. The effect of tailing is somewhat less dramatic for a continuous injection (cumulative concentration of a pulse). The breakthrough curve approaches asymptotically the input concentration (c_e) with the bulk of solute arising at t_A.

For slow exchange (large $\tau_{\alpha_0 D}$), most of the solute mass pulse flows in the mobile region, so that the peak arrival time coincides with the advective time (red arrow in Fig. 3). Fast exchange (shorter $\tau_{\alpha_0 D}$) allows equilibrating concentration in the mobile and immobile zones, so that the medium behaves as if the whole porosity was mobile. It is important to notice the above separation between fast and slow is relative to the advective transport time ($t_{Am} = L\phi_m/q$, where L is the travel distance of solute). If $t_A \gg \tau_\alpha$, the immobile region becomes accessible to the solute and the actual travel time reflects the total porosity ($t_{AT} = L\phi/q$, where $\phi = \phi_m + \phi_{im}$ is the total porosity). This effect is similar to retardation, and it is frequently stated that the impact of immobile zones is to retard the solute (e.g., Haggerty and Gorelick, 1995). In fact, the peak arrival for the $\tau_{\alpha_0 D} = 10^{-1}$ BTC in Fig. 3 (orange arrow) is retarded by a factor of 4, which reflects that $\phi_m + \phi_{im}$ equals $4\phi_m$. Note, however, that (1) this kind of retardation has nothing to do with adsorption or any other partitioning process (in fact, ϕs in our equations can be viewed as retention capacities for sorbing solutes), and (2) the apparent retardation associated to diffusion in immobile zones will be distance and flux dependent.

This kind of observations may explain why non-local models are less popular in unconsolidated, granular, aquifers than in fractured media. Fractured media with diffusion lengths of the order of meters will display residence times of the order $t_D = L^2/D = (10m)^2/10^{-10}m^2/s \cong 10^{12}s \cong 3.10^5 years$. That is, diffusion is never exhausted. Diffusion lengths in porous media are less than 1 cm, so that residence times in immobile zones will be of the order of $t_D = (10^{-2}m)^2/10^{-10}m^2/s = 10^6 s \sim 4$ *months*. This time may be relevant for tracer tests, where travel time is of a few days, but is too short for natural groundwater flow. Support for this kind of observations is provided by Guimerà and Carrera (2000). They observed that the "advective porosity" (i.e. the porosity derived from the peak arrival time) calculated from a broad collection of tracer tests in fractured rocks correlates with the peak arrival time. This implies that the apparent mobile porosity increases when the flow rate is reduced, which we take as indicative of fast immobile regions equilibrating with truly mobile zones. Increasing the travel time causes an increasing fraction of immobile regions to equilibrate with mobile zones, thus becoming effectively mobile.

Further insight into the behavior of conservative solutes can be gained from Fig. 3 (right), which displays the immobile concentration (color scale) versus distance and immobile residence time for $t_D = 300$. The figure might be considered somewhat misleading in that the vertical axis refers to immobile porosity associated to small residence times (recall pdf of immobile zones for a gamma distribution, Fig. 2) and not distance to the mobile zone. However, as shown in Fig. 3 the concentration in immobile regions is independent of their volumetric fraction. What Fig. 3 (right) shows is that concentrations in the immobile zones with short residence times (from $\tau_{\alpha D} = 10^{-2}$ to 10^1, much shorter than the dimensionless travel time of 300) are identical to concentrations in the mobile zone. On the other hand, concentration is negligible in the immobile zones whose residence time is much larger than travel time, for $\tau_{\alpha D}$ higher than 10^3 the concentration in the immobile zones is 0 even at the shorter distances. This might suggest that slow immobile regions might be neglected, whereas fast immobile regions might be lumped with the mobile domain. While this may be appropriate for inert tracers, it may not be suitable for reacting tracers because reactivity is usually higher in the immobile regions, certainly in the case of biofilms (Kone et al., 2014; Seifert and Engesgaard, 2007; Taylor and Jaffé, 1990), which motivates our work.

4.2. Single reaction system

In this case we consider two solutes, A and B, A is the only solute present in the inflow water while B is produced by the degradation of A.

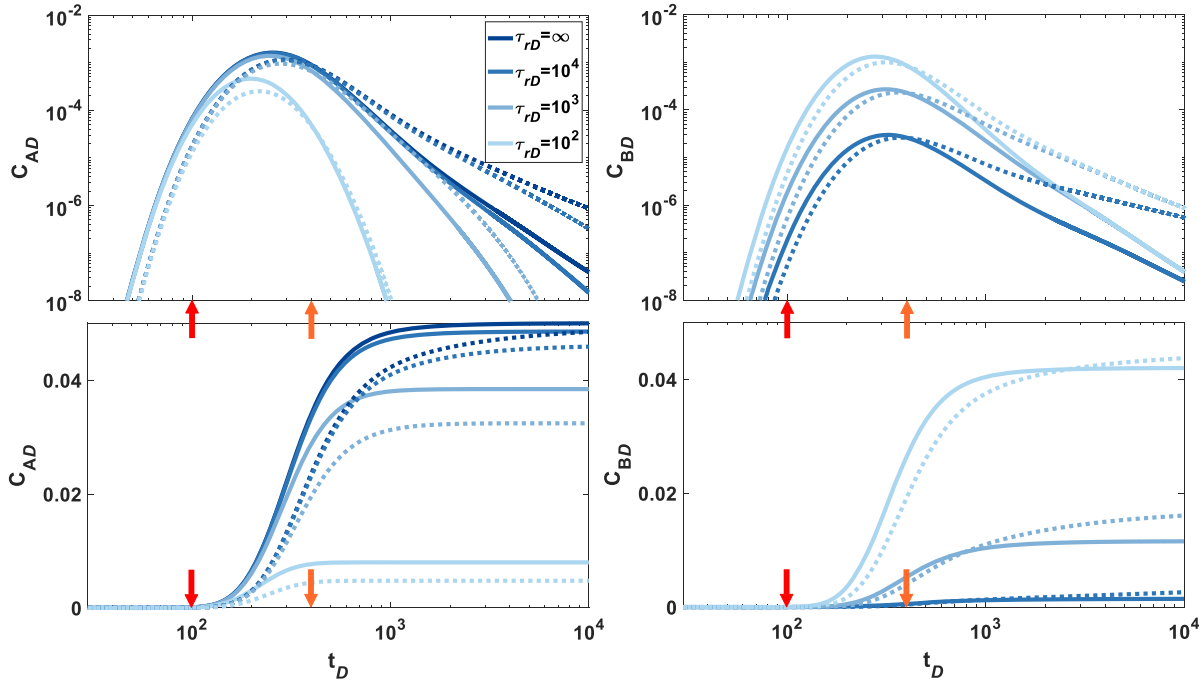

Fig. 4. Mobile (solid lines) and average immobile (dash lines) concentrations of species A (left column) and B (right column) versus time at $x_D = 100L_c$ in response to a pulse input (up row) and to a continuous injection (bottom row) for transport in a medium with a gamma distribution of residence times in immobile zones with $\beta = 1/2$, and $\tau_{\alpha_0 D} = 10$. Reaction times are uniformly distributed in immobile zones with $\tau_{rD} = \infty$, 10^4, 10^3 and 10^2. Species B is absent when no reaction occurs ($\tau_{rD} = \infty$).

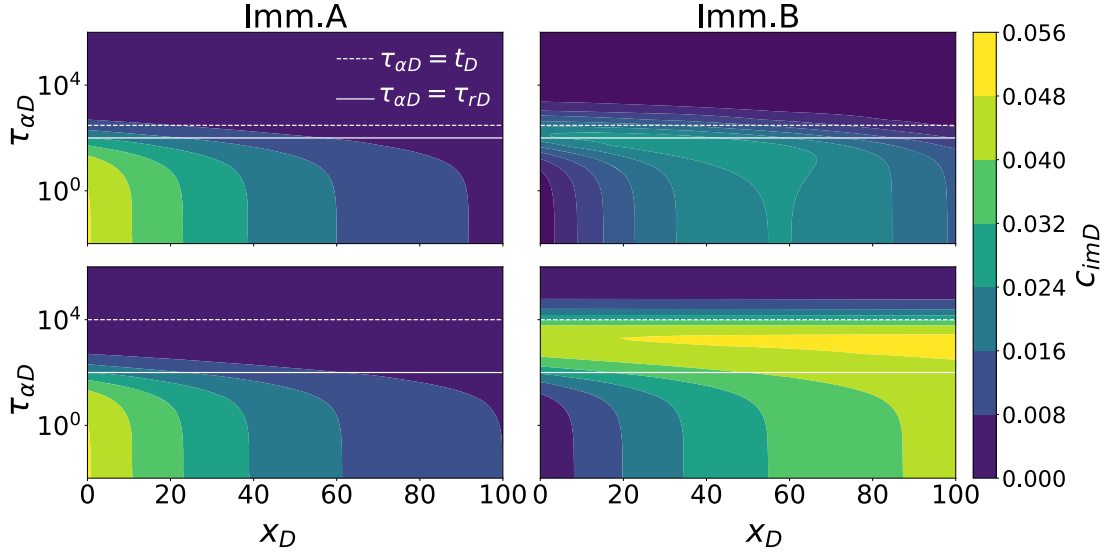

Fig. 5. Cumulative concentration profiles versus dimensionless distance and dimensionless residence times for species A (left) and B (right) at $t_D = 300$ (top), and 10000 (bottom) after continuous injection of A in a medium with a gamma distribution of residence times in immobile zones with $\beta = 1/2$, $\tau_{\alpha_0 D} = 10$. Reaction A→B occurs with a characteristic time $\tau_{rD} = 10^2$. The white solid lines indicate immobile zones whose residence times equals the reaction time, $\tau_{\alpha D} = \tau_{rD}$, and the white dash lines denote immobile zones whose residence times approximate the simulation time, $\tau_{\alpha D} = t_D$.

Concentrations of the two species in mobile and immobile zones for a pulse and a continuous injection are shown in Fig. 4 for several reaction times higher than the mean residence time. The situation is now more complicated than in the conservative transport case because three sets of characteristic times are involved (residence times in immobile zones, reaction times, and advective transport time). The first immediate observation, is that maximum concentrations of species A are reduced when the reaction rate is increased (i.e., when the characteristic reaction time is reduced). Note that BTC concentrations of A become negligible when reaction time is much smaller than transport time (i.e., for case of $\tau_{rD} = 10^2$, when transport time $t_D > 10^3$, that means $\tau_{rD} \ll t_D$, species A is almost reduced and cannot be detected).

The behavior of the distribution of concentrations in the immobile regions may be less intuitive (see Fig. 5). Concentration of the parent species, A, is negligible in immobile zones with residence time much larger than the reaction time ($\tau_{\alpha D} \gg \tau_{rD}$), because the solute diffusing into these zones is degraded before a significant concentration can build up. It is also negligible in zones where residence time is much larger than the simulation time (t_D) because almost no solute has diffused into these regions yet. On the other extreme, concentration in fast immobile

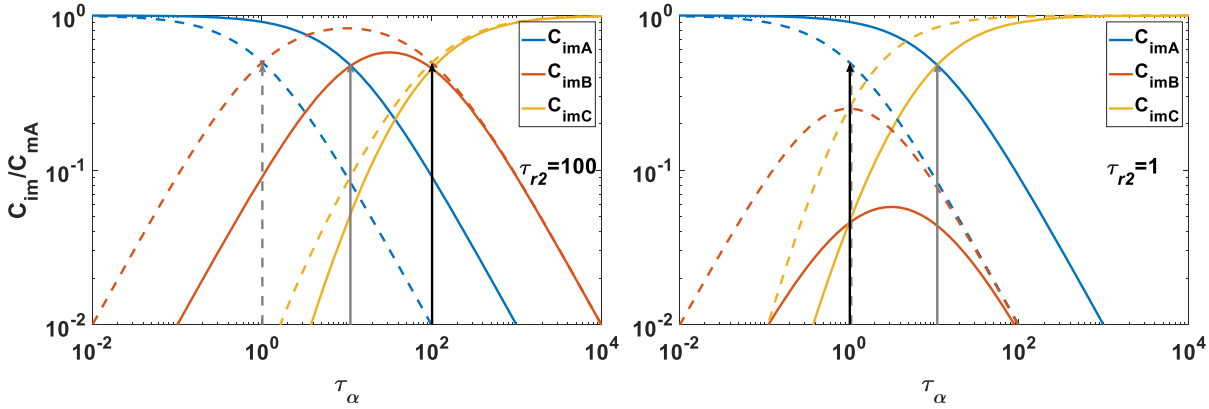

Fig. 6. Steady state concentrations of species A (blue), B (orange), and C (yellow) as a function of residence time in immobile zones, τ_α[T], assuming that mobile concentrations of B and C are zero. The first reaction time, τ_{r1} [T], for A→B transformation equals 10 (solid) and 1 (dash). The reaction time, τ_{r2} [T], for B→C reaction is 100 (left) and 1 (right). The corresponding reaction times are indicated by arrows.

regions is virtually equal to the mobile concentration, which suggests that these regions could be lumped with the mobile regions.

More interesting is the behavior of daughter species B, which is washed away from the mobile zone and fast immobile zones before it becomes significant. As a result, B concentrations are dominant in immobile zones whose residence time lies between the reaction time and the simulation time; Solute A has arrived at immobile zones with residence time shorter than t_D. At those immobile zones with residence time higher than reaction time, A has been transformed into B. This is the fundamental point to demonstrate that B has become localized in certain immobile zones, which motivates this work and is further analyzed for the case of sequential reactions.

4.3. Sequential reaction system

The sequential reaction case becomes increasingly complicated by the multiplicity of times involved. Therefore, we start by considering the steady state solution to the sequential reaction system for a generic immobile region that exchanges mass with the mobile zone. The governing equations are

$$\begin{aligned} 0 &= \alpha(c_{mA} - c_A) - k_1 c_A \\ 0 &= \alpha(c_{mB} - c_B) + k_1 c_A - k_2 c_B \\ 0 &= \alpha(c_{mC} - c_C) + k_2 c_B \end{aligned} \tag{26}$$

where we have dropped the dependence on x_D,t_D and $\tau_{\alpha D}$ for simplicity and because it is self-evident (i.e., $c_A = c_{im,A}(x_D,\tau_{\alpha D},t_D)$, $c_{mA} = c_{mA}(x_D,t_D)$, etc.). From Eq. (26), we can obtain the analytical solution of each species at steady state, as a function of the mobile concentrations:

$$\begin{aligned} c_A &= \frac{\alpha c_{mA}}{(\alpha + k_1)} \\ c_B &= \frac{\alpha c_{mB} + k_1 c_A}{(\alpha + k_2)} \\ c_C &= \frac{\alpha c_{mC} + k_2 c_B}{\alpha} \end{aligned} \tag{27}$$

These expressions become clearer when the concentrations of daughter products in the mobile zone can be neglected (i.e., near the input, assuming they are absent in the inflow, and that the advective flux is large) Assuming $c_{mB} = c_{mC} = 0$ in Eq. (27), we get

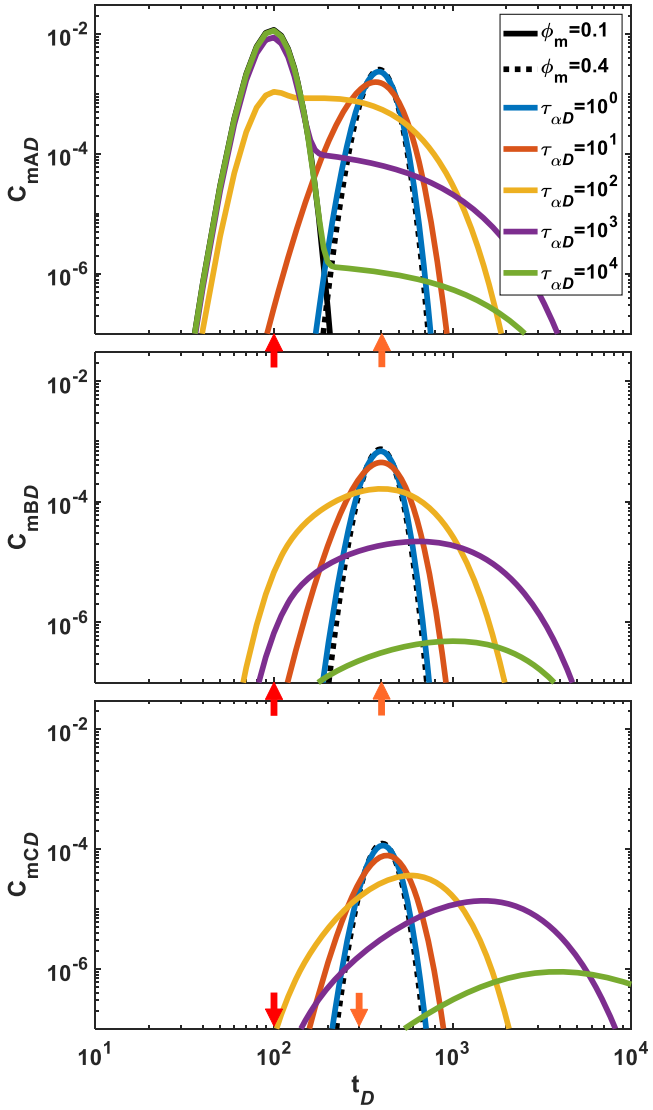

Fig. 7. Breakthrough curves of species A, B and C at $L = 100L_c$ with one immobile (color lines) zone for $\tau_{r1D} = \tau_{r2D} = 10^3$. The black solid line represents results with a mobile zone with $\phi_m = 0.1$ [-] and no reaction (in which case species B and C are never formed). The black dotted lines represent results with a mobile zone with $\phi_m = 0.4$ [-] and $\tau_{r1,mD} = \tau_{r2,mD} = 1333$ (i.e., $k_{1,m} = k_{2,m} = 0.0075$).

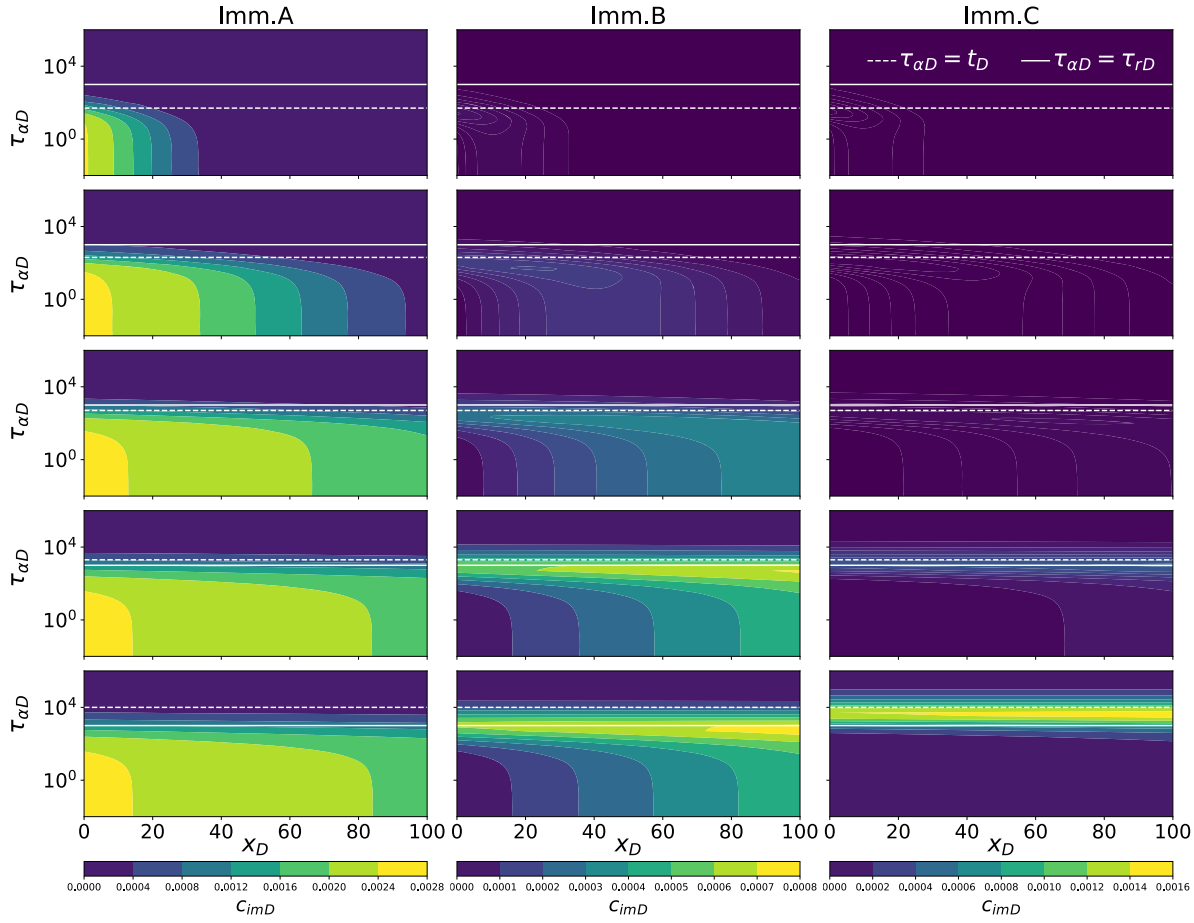

Fig. 8. Cumulative concentration profiles versus dimensionless distance and dimensionless residence times for species A (left), B (middle) and C (right) for $\tau_{r1D} = \tau_{r2D} = 10^3$ at $t_D = 50$, 200, 500, 2000 and 10000 from top to bottom. The medium is characterized by immobile zones of which the residence time follows a gamma distribution with $\beta = 1/2$, $\tau_{\alpha_0 D} = 10$.

$$\begin{aligned} \frac{c_A}{c_{mA}} &= \frac{\alpha}{(\alpha + k_1)} \\ \frac{c_B}{c_{mA}} &= \frac{\alpha k_1}{(\alpha + k_1)(\alpha + k_2)} \\ \frac{c_C}{c_{mA}} &= \frac{k_1 k_2}{(\alpha + k_1)(\alpha + k_2)} \end{aligned} \tag{28}$$

Fig. 6 displays the steady state concentrations of species A, B and C in immobile zones versus residence time ($\tau_\alpha = 1/\alpha$). Note that the sum of concentrations A, B and C equals one, which is the concentration of A in the inflow. This reflects the fact that this sum is conservative, because $r_A + r_B + r_C = -k_1 c_A + k_1 c_A - k_2 c_B + k_2 c_B = 0$ and the fact that at steady state the concentration of a conservative species in any immobile zone equals the mobile concentration. As can be observed, species A (blue), which is the only species present in the mobile zone, dominates immobile zones with residence times much smaller than the reaction time of the first reaction (say $\tau_\alpha < \tau_{r1}/10$). Therefore, immobile zones with residence times significantly lower than the first reaction characteristic time can effectively be considered as mobile. Species B (orange) dominates immobile zones with residence times between the two reaction times when $\tau_{r1} < \tau_{r2}$, but its concentration is negligible when $\tau_{r1} > \tau_{r2}$ (i.e., when its decay is faster than its production). Species C (yellow) dominates those immobile zones with residence times larger than the reaction time of the second reaction ($\tau_\alpha > \tau_{r2} = 1/k_2$). Thus, when the second reaction is also fast (right graph of Fig. 6), the concentration of the intermediate species (B) becomes small, and the two reactions could probably be lumped and species B neglected (provided it does not affect other reactions).

Results for the full transport case (A→B and B→C) are summarized in Fig. 7 and Fig. 8. Fig. 7 displays the BTCs for the transport conditions of Fig. 3 and Fig. 4, but only one immobile region to better isolate the effect of residence time. As in Fig. 7, when the exchange is slow, the BTC of species A (green and purple BTCs for $\tau_{\alpha_0 D} = 10^4$ and 10^3, respectively) overlaps with that of a conservative solute in the mobile zone (black line), except at the tail. The concentrations of B and C are very small (note the vertical axis).

The case of short residence times is also illustrative. The corresponding BTC (blue line) is virtually identical to the BTC (dotted black line) where all the porosity has been lumped as mobile. Obviously, the immobile zone reactions must be accounted for in this mobile (the effective reaction rate is derived in the Appendix A). That is, immobile regions with short residence time (compared to transport and reaction times, i.e., $\tau_{\alpha D} \ll t_D$, and $\tau_{\alpha D} \ll \tau_{rD}$) can be lumped and treated as mobile. The effective reaction rate in the case of Fig. 7 turns out to be, $k_{am} = k_{im}\phi_{im}/(\phi_{im} + \phi_m)$ (see Appendix A).

The most significant observation from the point of view of chemical localization derives from Fig. 8, which displays immobile regions concentrations as a function of space and residence time. This figure makes it clear that C concentrations are only relevant in immobile zones with residence times comparable to reaction times, regardless of the transport time. Therefore, the three sets of times (transport time, reaction time, and residence times) are relevant when deciding the appropriate discretization of residence times. Note that this result is consistent with that of Fig. 6. The second reaction tends to become localized in zones where the residence time is greater than the first reaction time, and the final daughter species, C, tends to concentrate in zones where the residence

time is greater than the second reaction time.

5. Conclusion

Several conclusions can be drawn from the modeling results presented in this work

1) Some reactions may occur in immobile regions that would not occur if the entire medium was mobile. This is not surprising when the mineral composition is different in each immobile zone, as was discussed by Soler-Segarra et al. (2016). What we show here is that, independently of the reactivity of mobile and immobile zones, the interplay between residence times and reaction times may cause some reactions to take place solely in the immobile zone. This will occur whenever residence time is larger than or comparable to reaction time, and both are much longer than the transport time. It goes without saying that immobile zone reactions will be enhanced if reactivity in immobile zones is higher than in the mobile zone. This is the case for biofilms, where microbial mediated degradation reactions concentrate.
2) Regardless of reaction rates, concentrations in the fast immobile zones (i.e., zones where $\tau_\alpha \ll t_D = L\phi/q$) will tend to equilibrate with mobile concentrations. Therefore, little is gained by representing them explicitly in a model. All fast exchange immobile zones can be lumped into the mobile zone, provided that the reaction rates are modified by the porosity ratio. In general, the corrected reaction rate will depend on both the actual immobile reaction rate and the residence time distribution in immobile zones. But this latter dependence becomes negligible when residence time is much smaller than the reaction time.
3) Similarly, very slow immobile zones ($\tau_\alpha \gg t_D$) can be ignored because little mass will diffuse into them. Note that this conclusion is more relevant for laboratory experiments or short tracer tests, where transport times are moderate. Under natural conditions, transport time can be very long (many years), so that most immobile zones are indeed accessible.
4) The time and space required for secondary species and reactions to build up may be large. This finding runs contrary to the frequent view of searching for metabolites and secondary species near the sources of parent species. Instead, they may tend to concentrate in isolated zones (i.e., with long residence times) at a distance from the source.

CRediT authorship contribution statement

Jingjing Wang: Conceptualization, Methodology, Software, Validation, Formal analysis, Investigation, Writing – original draft, Writing – review & editing, Visualization. **Jesus Carrera:** Conceptualization, Methodology, Validation, Formal analysis, Resources, Writing – original draft, Writing – review & editing, Visualization, Supervision, Funding acquisition. **Maarten W. Saaltink:** Conceptualization, Validation, Formal analysis, Writing – original draft, Writing – review & editing, Visualization, Supervision. **Cristina Valhondo:** Conceptualization, Validation, Formal analysis, Writing – original draft, Writing – review & editing, Visualization, Supervision.

Declaration of Competing Interest

The authors declare that they have no known competing financial interests or personal relationships that could have appeared to influence the work reported in this paper.

Acknowledgements

The authors acknowledge the financial support of project NITREM (European Union, European Institute of Innovation and Technology, project number 17013, PA2021/EIT/EIT Raw Materials GA2021 EIT RM) and the project RESTORA (Agència Catalana de l'Aigua, ACA210/18/0040). Additional funding was obtained from the Generalitat de Catalunya (2017 SGR1485) and the Spanish Ministry of Science and Innovation (Centre of Excellence Severo-Ochoa, CSIC-IDAEA, CEX2018–000794-S).

Appendix A

The objective of this appendix is to find an effective reaction rate in the mobile zone for cases when residence time in the immobile zone is much smaller than the reaction time. Such fast exchanging immobile zones can be lumped in the mobile zone, but their reactions also need to be included in the mobile zone. To this end, we consider a simplified steady state mass balance in the mobile zone, where the advection and dispersion terms are substituted by $w(c_{ex} - c_m)$, where w is the flow rate per unit volume of medium that enters the mobile zone with concentration c_{ex} (and leaves with concentration c_m). Under steady-state conditions, mass balance reads:

$$\phi_m \frac{dc_m}{dt} = w(c_{ex} - c_m) - \sum_j^{N_{im}} \phi_{im}^j \alpha_{im}^j \left[c_m - c_{im}^j\right] - \phi_m \lambda_m c_m = 0 \tag{A1}$$

where ϕ_m [-] and ϕ_{im}^j [-] are the retention capacities of mobile and j immobile zone, respectively; c_m [ML^{-3}] and c_{im}^j [ML^{-3}] are concentrations in the mobile and immobile zone, which are expressed as mass per unit volume of mobile and immobile water, respectively; α_{im}^j [T^{-1}] is the mass exchange rate between mobile and jth immobile zone; λ_m[$ML^{-3}T^{-1}$] is the rate constant for degradation reactions in the mobile zone and corresponds to the mass removed by reactions in the mobile zone per unit volume of mobile water per unit time.

Mass balance in each immobile zone is given by

$$\frac{dc_{im}^j}{dt} = \alpha_{im}^j \left[c_m - c_{im}^j\right] - \lambda_{im}^j c_{im}^j = 0 \tag{A2}$$

Solving Eq. (A2) for c_{im}^j, yields

$$c_{im}^j = \frac{\alpha_{im}^j c_m}{\alpha_{im}^j + \lambda_{im}^j} \tag{A3}$$

Substituting c_{im}^j into Eq. (A1) and solving for c_m yields

$$c_m = \frac{w}{w + \sum_j^{N_{im}} \frac{\phi_{im}^j \alpha_{im}^j \lambda_{im}^j}{\alpha_{im}^j + \lambda_{im}^j} + \phi_m \lambda_m} c_{ex} \tag{A4}$$

This equation can also be used for the case in which all (in general a subset of) immobile zones are lumped into the mobile zone, which we denote with subscript *am* (all mobile)

$$c_{am} = \frac{w}{w + \phi_{am} \lambda_{am}} c_{ex} \tag{A5}$$

Comparing Eqs. (A4) and Eq. (A5), it is clear that the solutions are identical if

$$\phi_{am} \lambda_{am} = \sum_j^{N_{im}} \frac{\phi_{im}^j \alpha_{im}^j \lambda_{im}^j}{\alpha_{im}^j + \lambda_{im}^j} + \phi_m \lambda_m \tag{A6}$$

Recalling that $\phi_{im}^j = p^j \phi_{im}$ and that $\phi_{am} = \phi_{im} + \phi_m$, gives

$$\lambda_{am} = \frac{\phi_{im}}{\phi_{im} + \phi_m} \sum_j^{N_{im}} \frac{p^j \alpha_{im}^j \lambda_{im}^j}{\alpha_{im}^j + \lambda_{im}^j} + \frac{\phi_{im}}{\phi_{im} + \phi_m} \lambda_m \tag{A7}$$

In the case discussed in the text, $\lambda_m = 0$, $\alpha_{im}^j \gg \lambda_{im}^j$, and all $\lambda_{im}^j = \lambda_{im}$, so that $\sum_j p^j = 1$ and

$$\lambda_{am} = \frac{\phi_{im} \lambda_{im}}{\phi_{im} + \phi_m} \tag{A8}$$

References

Adams, E.E., Gelhar, L.W., 1992. Field study of dispersion in a heterogeneous aquifer: 2. Spatial moments analysis. Water Resour. Res. https://doi.org/10.1029/92WR01757.

Agrawal, P., Mascini, A., Bultreys, T., Aslannejad, H., Wolthers, M., Cnudde, V., Butler, I. B., Raoof, A., 2021. The impact of pore-throat shape evolution during dissolution on carbonate rock permeability: pore network modeling and experiments. Adv. Water Resour. 155 https://doi.org/10.1016/j.advwatres.2021.103991.

Babaei, M., Islam, A., 2018. Convective-Reactive CO2 Dissolution in Aquifers With Mass Transfer With Immobile Water. Water Resour. Res. https://doi.org/10.1029/2018WR023150.

Babey, T., de Dreuzy, J.R., Casenave, C., 2015. Multi-Rate Mass Transfer (MRMT) models for general diffusive porosity structures. Adv. Water Resour. https://doi.org/10.1016/j.advwatres.2014.12.006.

Babey, T., de Dreuzy, J.R., Rapaport, A., Rojas-Palma, A., 2017. Inherent relevance of MRMT models to concentration variance and mixing-induced reactivity. Adv. Water Resour. https://doi.org/10.1016/j.advwatres.2017.09.024.

Battiato, I., Tartakovsky, D.M., Tartakovsky, A.M., Scheibe, T., 2009. On breakdown of macroscopic models of mixing-controlled heterogeneous reactions in porous media. Adv. Water Resour. 32 https://doi.org/10.1016/j.advwatres.2009.08.008.

Bellin, D.L., Sakhtah, H., Rosenstein, J.K., Levine, P.M., Thimot, J., Emmett, K., Dietrich, L.E.P., Shepard, K.L., 2014. Integrated circuit-based electrochemical sensor for spatially resolved detection of redox-active metabolites in biofilms. Nat. Commun. 5 https://doi.org/10.1038/ncomms4256.

Benson, D.A., Meerschaert, M.M., 2009. A simple and efficient random walk solution of multi-rate mobile/immobile mass transport equations. Adv. Water Resour. https://doi.org/10.1016/j.advwatres.2009.01.002.

Benson, D.A., Wheatcraft, S.W., Meerschaert, M.M., 2000. The fractional-order governing equation of Levy motion. Water Resour. Res. https://doi.org/10.1029/2000WR900032.

Berkowitz, B., Cortis, A., Dentz, M., Scher, H., 2006. Modeling Non-fickian transport in geological formations as a continuous time random walk. Rev. Geophys. https://doi.org/10.1029/2005RG000178.

Berkowitz, B., Scher, H., 2009. Exploring the nature of non-Fickian transport in laboratory experiments. Adv. Water Resour. https://doi.org/10.1016/j.advwatres.2008.05.004.

Berkowitz, B., Scher, H., 1998. Theory of anomalous chemical transport in random fracture networks. Phys. Rev. E - Stat. Physics, Plasmas, Fluids, Relat. Interdiscip. Top. https://doi.org/10.1103/PhysRevE.57.5858.

Carrera, J., 1993. An overview of uncertainties in modelling groundwater solute transport. J. Contam. Hydrol. 13, 23–48. https://doi.org/10.1016/0169-7722(93)90049-X.

Carrera, J., Saaltink, M.W., Soler-Sagarra, J., Jingjing, W., Valhondo, C., 2022. Reactive Transport: a Review of Basic Concepts with Emphasis on Biochemical Processes. Energies 15. https://doi.org/10.3390/en15030925.

Carrera, J., Sánchez-Vila, X., Benet, I., Medina, A., Galarza, G., Guinerà, J., 1998. On matrix diffusion: formulations, solution methods and qualitative effects. Hydrogeol. J. https://doi.org/10.1007/s100400050143.

Cirpka, O.A., Chiogna, G., Rolle, M., Bellin, A., 2015. Transverse mixing in three-dimensional nonstationary anisotropic heterogeneous porous media. Water Resour. Res. 51 https://doi.org/10.1002/2014WR015331.

De Dreuzy, J.R., Rapaport, A., Babey, T., Harmand, J., 2013. Influence of porosity structures on mixing-induced reactivity at chemical equilibrium in mobile/immobile Multi-Rate Mass Transfer (MRMT) and Multiple INteracting Continua (MINC) models. Water Resour. Res. https://doi.org/10.1002/2013WR013808.

Deng, H., Spycher, N., 2019. Modeling reactive transport processes in fractures. Rev. Mineral. Geochemistry 85. https://doi.org/10.2138/rmg.2019.85.3.

Dentz, M., Berkowitz, B., 2003. Transport behavior of a passive solute in continuous time random walks and multirate mass transfer. Water Resour. Res. https://doi.org/10.1029/2001WR001163.

Dentz, M., Cortis, A., Scher, H., Berkowitz, B., 2004. Time behavior of solute transport in heterogeneous media: transition from anomalous to normal transport. Adv. Water Resour. https://doi.org/10.1016/j.advwatres.2003.11.002.

Dentz, M., Gouze, P., Carrera, J., 2011. Effective non-local reaction kinetics for transport in physically and chemically heterogeneous media. J. Contam. Hydrol. 120–121. https://doi.org/10.1016/j.jconhyd.2010.06.002.

Dentz, M., Kang, P.K., Le Borgne, T., 2015. Continuous time random walks for non-local radial solute transport. Adv. Water Resour. https://doi.org/10.1016/j.advwatres.2015.04.005.

Donado, L.D., Sanchez-Vila, X., Dentz, M., Carrera, J., Bolster, D., 2009. Multicomponent reactive transport in multicontinuum media. Water Resour. Res. https://doi.org/10.1029/2008WR006823.

Fernandez-Garcia, D., Sanchez-Vila, X., 2015. Mathematical equivalence between time-dependent single-rate and multiratemass transfer models. Water Resour. Res. 51, 3166–3180. https://doi.org/10.1016/0022-1694(68)90080-2.

Gouze, P., Melean, Y., Le Borgne, T., Dentz, M., Carrera, J., 2008. Non-Fickian dispersion in porous media explained by heterogeneous microscale matrix diffusion. Water Resour. Res. https://doi.org/10.1029/2007WR006690.

Guimerà, J., Carrera, J., 2000. A comparison of hydraulic and transport parameters measured in low- permeability fractured media. J. Contam. Hydrol. 41, 261–281. https://doi.org/10.1016/S0169-7722(99)00080-7.

Haggerty, R., Gorelick, S.M., 1995. Multiple-Rate Mass Transfer for Modeling Diffusion and Surface Reactions in Media with Pore-Scale Heterogeneity. Water Resour. Res. https://doi.org/10.1029/95WR10583.

Haggerty, R., Harvey, C.F., Von Schwerin, C.F., Meigs, L.C., 2004. What controls the apparent timescale of solute mass transfer in aquifers and soils? A comparison of experimental results. Water Resour. Res. https://doi.org/10.1029/2002WR001716.

Haggerty, R., McKenna, S.A., Meigs, L.C., 2000. On the late-time behavior of tracer test breakthrough curves. Water Resour. Res. https://doi.org/10.1029/2000WR900214.

Kitanidis, P.K., 1988. Prediction by the method of moments of transport in a heterogeneous formation. J. Hydrol. https://doi.org/10.1016/0022-1694(88)90111-4.

Kone, T., Golfier, F., Orgogozo, L., Oltéan, C., Lefèvre, E., Block, J.C., Buès, M.A., 2014. Impact of biofilm-induced heterogeneities on solute transport in porous media. Water Resour. Res. https://doi.org/10.1002/2013WR015213.

Levy, M., Berkowitz, B., 2003. Measurement and analysis of non-Fickian dispersion in heterogeneous porous media. J. Contam. Hydrol. https://doi.org/10.1016/S0169-7722(02)00204-8.

Li, L., Steefel, C.I., Yang, L., 2008. Scale dependence of mineral dissolution rates within single pores and fractures. Geochim. Cosmochim. Acta 72. https://doi.org/10.1016/j.gca.2007.10.027.

Lichtner, P.C., Kang, Q., 2007. Upscaling pore-scale reactive transport equations using a multiscale continuum formulation. In: Water Resources Research. https://doi.org/10.1029/2006WR005664.

Luquot, L., Gouze, P., Niemi, A., Bensabat, J., Carrera, J., 2016. CO2-rich brine percolation experiments through Heletz reservoir rock samples (Israel): role of the flow rate and brine composition. Int. J. Greenh. Gas Control. https://doi.org/10.1016/j.ijggc.2015.10.023.

Marseguerra, M., Zoia, A., 2008. Monte Carlo evaluation of FADE approach to anomalous kinetics. Math. Comput. Simul. https://doi.org/10.1016/j.matcom.2007.03.001.

Massoudieh, A., Dentz, M., 2020. Upscaling non-linear reactive transport in correlated velocity fields. Adv. Water Resour. 143 https://doi.org/10.1016/j.advwatres.2020.103680.

Molins, S., Knabner, P., 2019. Multiscale Approaches in Reactive Transport Modeling. Rev. Mineral. Geochemistry 85, 27–48. https://doi.org/10.2138/rmg.2019.85.2.

Neuman, S.P., Tartakovsky, D.M., 2009. Perspective on theories of non-Fickian transport in heterogeneous media. Adv. Water Resour. https://doi.org/10.1016/j.advwatres.2008.08.005.

Pruess, K., Narasimhan, T.N., 1985. Practical method for modeling fluid and heat flow in fractured porous media. Soc. Pet. Eng. J.

Rapaport, A., Rojas-Palma, A., De Dreuzy, J.R., Ramirez, H.C., 2017. Equivalence of Finite Dimensional Input-Output Models of Solute Transport and Diffusion in Geosciences. IEEE Trans. Automat. Contr. https://doi.org/10.1109/TAC.2017.2701150.

Saaltink, M.W., Carrera, J., Ayora, C., 2001. On the behavior of approaches to simulate reactive transport. J. Contam. Hydrol. 48 https://doi.org/10.1016/S0169-7722(00)00172-8.

Salamon, P., Fernàndez-Garcia, D., Gómez-Hernández, J.J., 2006. Modeling mass transfer processes using random walk particle tracking. Water Resour. Res. https://doi.org/10.1029/2006WR004927.

Scheibe, T.D., Fang, Y., Murray, C.J., Roden, E.E., Chen, J., Chien, Y.J., Brooks, S.C., Hubbard, S.S., 2006. Transport and biogeochemical reaction of metals in a physically and chemically heterogeneous aquifer. Geosphere 2. https://doi.org/10.1130/GES00029.1.

Schumer, R., Benson, D.A., Meerschaert, M.M., Baeumer, B., 2003a. Multiscaling fractional advection-dispersion equations and their solutions. Water Resour. Res. 39 https://doi.org/10.1029/2001WR001229.

Schumer, R., Benson, D.A., Meerschaert, M.M., Baeumer, B., 2003b. Fractal mobile/immobile solute transport. Water Resour. Res. https://doi.org/10.1029/2003WR002141.

Seifert, D., Engesgaard, P., 2007. Use of tracer tests to investigate changes in flow and transport properties due to bioclogging of porous media. J. Contam. Hydrol. 93 https://doi.org/10.1016/j.jconhyd.2007.01.014.

Silva, O., Carrera, J., Dentz, M., Kumar, S., Alcolea, A., Willmann, M., 2009. A general real-time formulation for multi-rate mass transfer problems. Hydrol. Earth Syst. Sci. https://doi.org/10.5194/hess-13-1399-2009.

Soler-Sagarra, J., Luquot, L., Martínez-Pérez, L., Saaltink, M.W., De Gaspari, F., Carrera, J., 2016. Simulation of chemical reaction localization using a multi-porosity reactive transport approach. Int. J. Greenh. Gas Control. https://doi.org/10.1016/j.ijggc.2016.01.026.

Soler-Sagarra, J., Saaltink, M.W., Nardi, A., De Gaspari, F., Carrera, J., 2022. Water Mixing Approach (WMA) for reactive transport modeling. Adv. Water Resour. 161, 104131 https://doi.org/10.1016/J.ADVWATRES.2022.104131.

Steefel, C.I., DePaolo, D.J., Lichtner, P.C., 2005. Reactive transport modeling: an essential tool and a new research approach for the Earth sciences. Earth Planet. Sci. Lett. 240 https://doi.org/10.1016/j.epsl.2005.09.017.

Taylor, S.W., Jaffé, P.R., 1990. Biofilm growth and the related changes in the physical properties of a porous medium: 3. Dispersivity and model verification. Water Resour. Res. https://doi.org/10.1029/WR026i009p02171.

Tian, H., Xu, T., Zhu, H., Yang, C., Ding, F., 2019. Heterogeneity in mineral composition and its impact on the sealing capacity of caprock for a CO 2 geological storage site. Comput. Geosci. 125 https://doi.org/10.1016/j.cageo.2019.01.015.

Valhondo, C., Carrera, J., Martínez-Landa, L., Wang, J., Amalfitano, S., Levantesi, C., Diaz-Cruz, M.S., 2020. Reactive barriers for renaturalization of reclaimed water during soil aquifer treatment. Water (Switzerland). https://doi.org/10.3390/W12041012.

Valocchi, A.J., 1985. Validity of the Local Equilibrium Assumption for Modeling Sorbing Solute Transport Through Homogeneous Soils. Water Resour. Res. https://doi.org/10.1029/WR021i006p00808.

Wang, J., Carrera, J., Saaltink, M.W., Valhondo, C., 2022. A general and efficient numerical solution of reactive transport with multirate mass transfer. Comput. Geosci. 158, 104953 https://doi.org/10.1016/j.cageo.2021.104953.

Wang, P.P., Zheng, C., Gorelick, S.M., 2005. A general approach to advective-dispersive transport with multirate mass transfer. Adv. Water Resour. https://doi.org/10.1016/j.advwatres.2004.10.003.

Willmann, M., Carrera, J., Sánchez-Vila, X., 2008. Transport upscaling in heterogeneous aquifers: what physical parameters control memory functions? Water Resour. Res. https://doi.org/10.1029/2007WR006531.

Willmann, M., Carrera, J., Sanchez-Vila, X., Silva, O., Dentz, M., 2010. Coupling of mass transfer and reactive transport for nonlinear reactions in heterogeneous media. Water Resour. Res. 46 https://doi.org/10.1029/2009WR007739.

Yeh, G.T., Tripathi, V.S., 1989. A critical evaluation of recent developments in hydrogeochemical transport models of reactive multichemical components. Water Resour. Res. 25 https://doi.org/10.1029/WR025i001p00093.